SUPPLEMENTARY INFORMATION

One-step Ethylene Purification from Ternary Mixtures by an Ultramicroporous Material with Synergistic Binding Centers

Xingye Li,† Qi Ding,† Jia Liu, Lihui Dong, Xingzhen Qin, Liqin Zhou, Zhenxia Zhao, Hongbing Ji, Sui Zhang,* and Kungang Chai*

Materials

All the chemicals were obtained from commercial resources and used as received without any further purification. $Co(OAc)_2 \cdot 4H_2O$ (> 99%) was purchased from Damas-Beta, citric acid monohydrate (AR, ≥ 99.5%) and KOH (RG, ≥ 99.0%) were purchased from General-Reagent.

Synthesis of UTSA-16

UTSA-16 was synthesized according to a reported method.[1] A mixture containing 1 mmol of $Co(OAc)_2 \cdot 4H_2O$, 1 mmol of citric acid monohydrate, 3 mmol of KOH, 2.5 mL of H_2O, and 2.5 mL of ethanol was added to a Teflon tube, then sealed and placed in an oven with a temperature of 120°C for 48 hours, and then slowly cooled to room temperature. The violet prismatic samples was collected by filtration, then washed with ethyl ether and dried in air. The sample was heated at 90°C under high vacuum for 24 h to obtain the activated UTSA-16.

Adsorption isotherm measurement

The adsorption isotherms were measured on the instrument of Micromeritics ASAP 2460. Before each measurement, about 100 mg of UTSA-16 was loaded into a glass analysis tube and heated at 90°C for 12 h under a high vacuum (< 7 μmHg). The sample was backfilled with N_2 before transferred to the analysis port, where it was evacuated for another 60 min before the analysis started.

Powder X-ray diffraction analysis

Powder X-ray diffraction (PXRD) patterns of UTSA-16 were collected using a BRUKER D8 Discover diffractometer (Cu Kα λ = 1.540598 Å) under 40 kV and 40 mA. The range of 2θ was from 5° to 50°. In situ PXRD patterns were collected with a chamber holding the sample, which was firstly activated under 120°C for 30 min. After cooled to room temperature, a flow of single gas was introduced into the chamber with a rate of 3 mL min^{-1} until the pressure reached 100 kPa. The XRD pattern was collected every 15 min. Rietveld refinement was performed on the PXRD data obtained under 100 kPa using the Reflex Module in *Materials Studio* software. The ligand molecule and the gas molecule were both treated as rigid bodies during the Rietveld refinements, with the molecule orientation and center of mass freely refined. Final refinement on the positions/orientations of the rigid bodies, thermal factors, occupancies, lattice parameters, background, and profiles converged with satisfactory *R*-factors.

Energy dispersive X-ray spectrometer analyses

The surface morphology of UTSA-16 was observed by field emission scanning electron microscopy (TESCAN MIRA LMS, Czech Republic), and the corresponding energy dispersive X-ray (EDX) spectrometer analyses were performed by a Oxford Xplore 30 EDX detection system.

Thermal gravimetric analysis

Thermal gravimetric analysis was performed on a thermal analyzer instrument (HTG-1/2) at a heating rate of 10 ºC min^{-1} up to 800 ºC under flowing nitrogen atmosphere. The amount of sample used during the tests was 10 (± 2) mg.

In situ Fourier transform infrared spectroscopy

The in situ Fourier transform infrared (FTIR) spectra were recorded using a FTIR spectrometer (Nicolet IS50). A vaccum cell is placed in the sample compartment of the infrared spectrometer with the sample at the focal point of the beam. The cell is connected to different gas lines and a vaccum line for evacuation. Prior to each test, the sample (*ca*. 100 mg) was placed in a vaccum cell and pretreated under high vacuum condition at 90°C for activation, and then cooled to room temperature for recording reference spectrum. Single gas (C_2H_2, CO_2, or C_2H_4) was introduced into the cell and the spectra were recorded during the gas exposure untill 30 min.

Calculation of IAST selectivity and separation potential

The adsorption isotherms of C_2H_2 and CO_2 were fitted using a dual-site Langmuir-Freundlich model

$$q = q_{mA}\frac{b_A p^{c_A}}{1 + b_A p} + q_{mB}\frac{b_B p^{c_B}}{1 + b_B p} \quad (1)$$

Here, p is the pressure of the bulk gas at equilibrium with the adsorbed phase (kPa), q is the adsorbed amount per mass of adsorbent (mmol g^{-1}), q_{mA} and q_{mB} are the saturation capacities of site A and B (mmol g^{-1}), b_A and b_B are the affinity coefficients of site A and B (kPa^{-1}), and c_A and c_b represent the deviations from an ideal homogeneous surface.

The adsorption isotherm of C_2H_4 was fitted using a single-site Langmuir- Freundlich model

$$q = q_{mA}\frac{b_A p^{c_A}}{1 + b_A p} \quad (2)$$

The adsorption selectivity is further calculated by the following equation

$$S_{ads} = \frac{q_1/q_2}{p_1/p_2} \quad (3)$$

q_1 and q_2 are the molar loadings in the adsorbed phase in equilibrium with the bulk gas phase with partial pressures p_1 and p_2.

Calculation of Q_{st}

The adsorption isotherms of C_2H_2, CO_2, and C_2H_4 measured at different temperatures (273 and 298 K) were firstly fitted with a Virial-type expression

$$\ln p = \ln n + \frac{1}{T}\sum_{i=0}^{c} a_i n^i + \sum_{j=0}^{d} b_j n^j \quad (4)$$

Here, p represents the pressure in mmHg, n represents the gas uptake in mg g^{-1}, T represents the temperature in Kelvin, a_i and b_i are Virial coefficients independent of temperature, c and d are the numbers of coefficients required to adequately describe the isotherms.

The Virial coefficients from a_0 to a_c were then used to calculate the isosteric heat of adsorption for a single gas according to the following expression

$$Q_{st} = -R\sum_{i=0}^{c} a_i n^i \qquad (5)$$

Breakthrough experiment

The breakthrough experiments were conducted on a home-built dynamic gas breakthrough equipment. In a typical procedure, a stainless-steel column (Φ 4.6 × 100 mm) packed with 1.8 g of UTSA-16 was firstly activated by purge with a flow of He (5 mL min^{-1}) at 90°C for 12 h. Gas mixture (C_2H_2/C_2H_4, CO_2/C_2H_4, or C_2H_2/ CO_2/C_2H_4 mixture) was then introduced into the column at a constant rate under 298 K and 1 bar. The concentration of the gas eluted from the outlet was detected by chromatography (GC-2018, SHIMADZU) with the thermal conductivity detector TCD. After the breakthrough experiment, the column was regenerated by purge with He at 90°C.

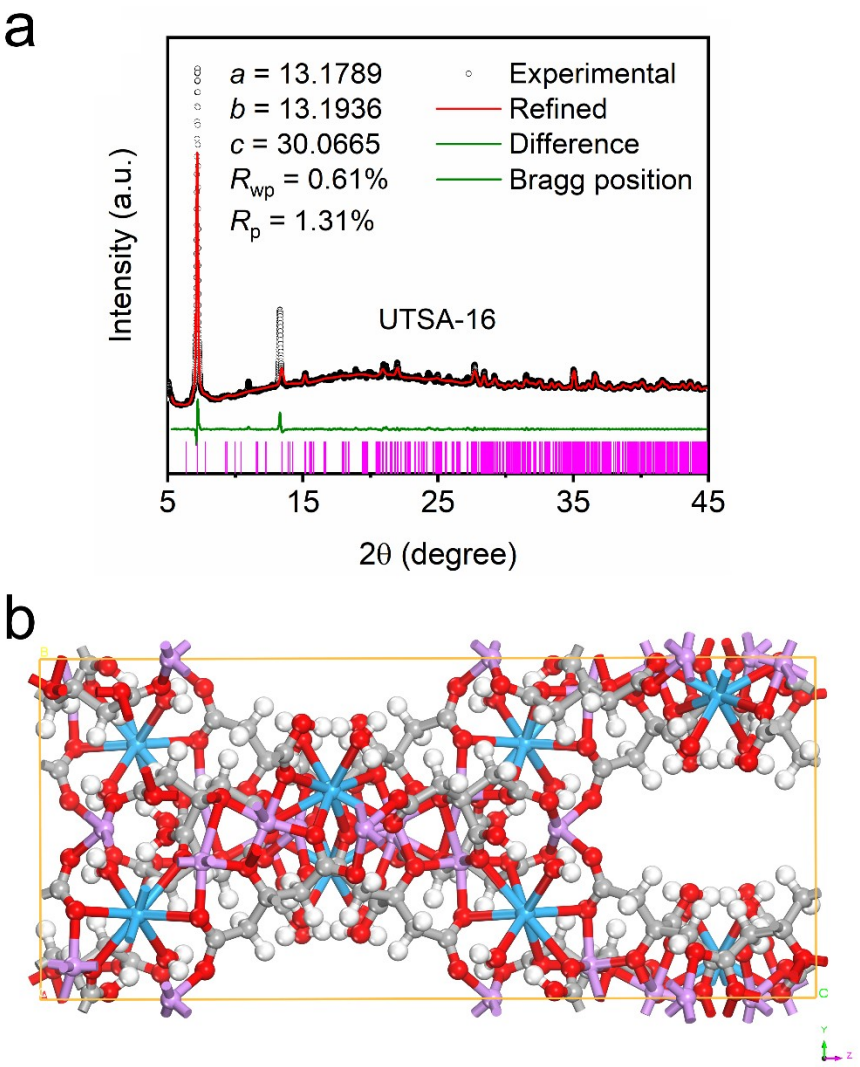

Figure S1. (a) Experimental in situ PXRD pattern and refined PXRD pattern of UTSA-16. (b) The refiend structure of UTSA-16 (color code: Co, lavender; K, blue; C, gray; H, white; O, red).

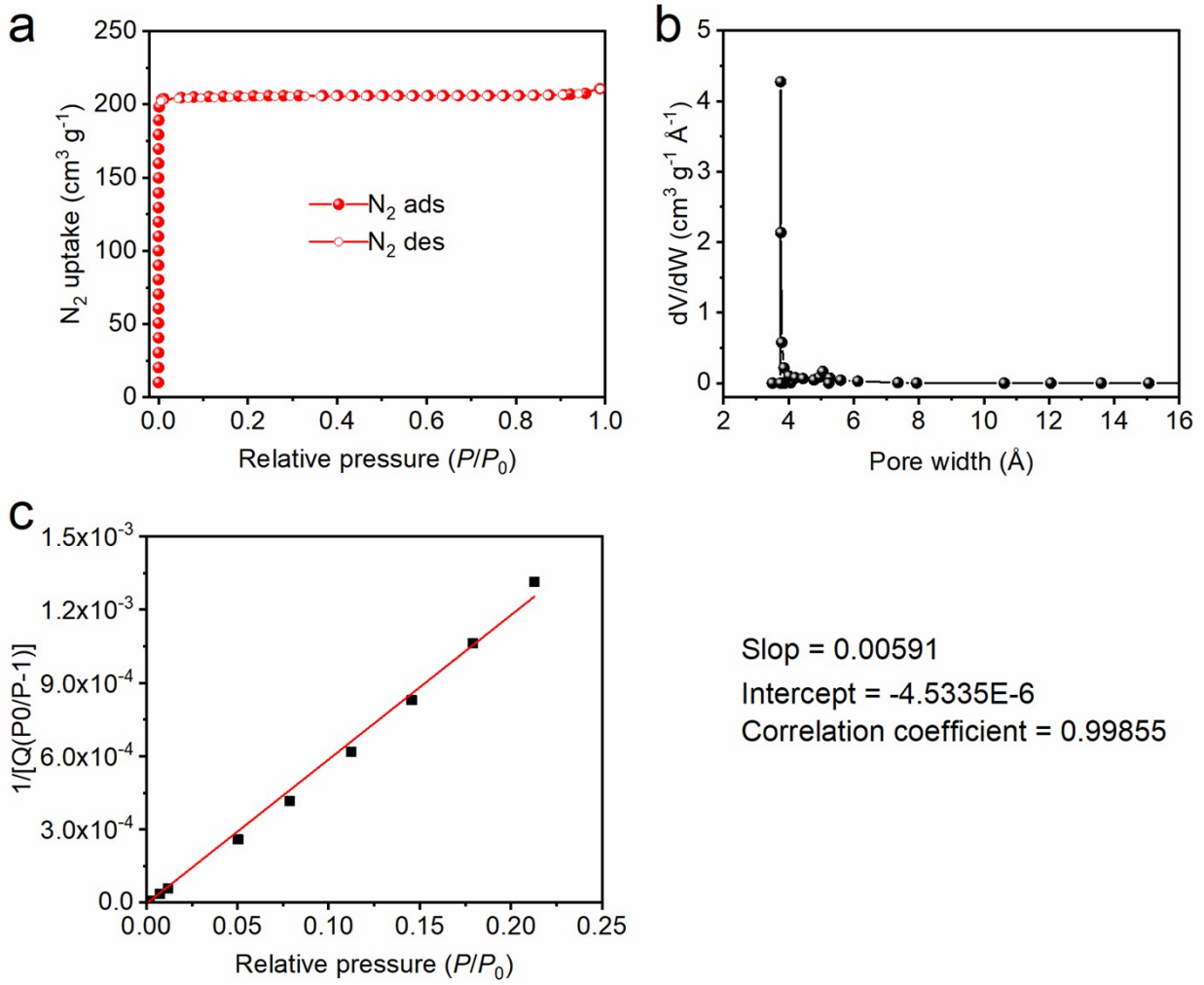

Figure S2. (a) Adsorption isotherm of N_2 at 77 K on UTSA-16. (b) Horvath–Kawazoe (HK) pore size distrobution of UTSA-16 derived from the N_2 adsorption isotherm. (c) BET surface area fit for UTSA-16 from 77 K N_2 adsorption isotherm.

The BET surface area calculated from the N_2 adsorption isotherms in the pressure range of P/P_0 = 0.002-0.21 is 737.2 m^2 g^{-1}.
The total pore volume calculated from the N_2 adsorption isotherms is 0.326 cm^3 g^{-1}.

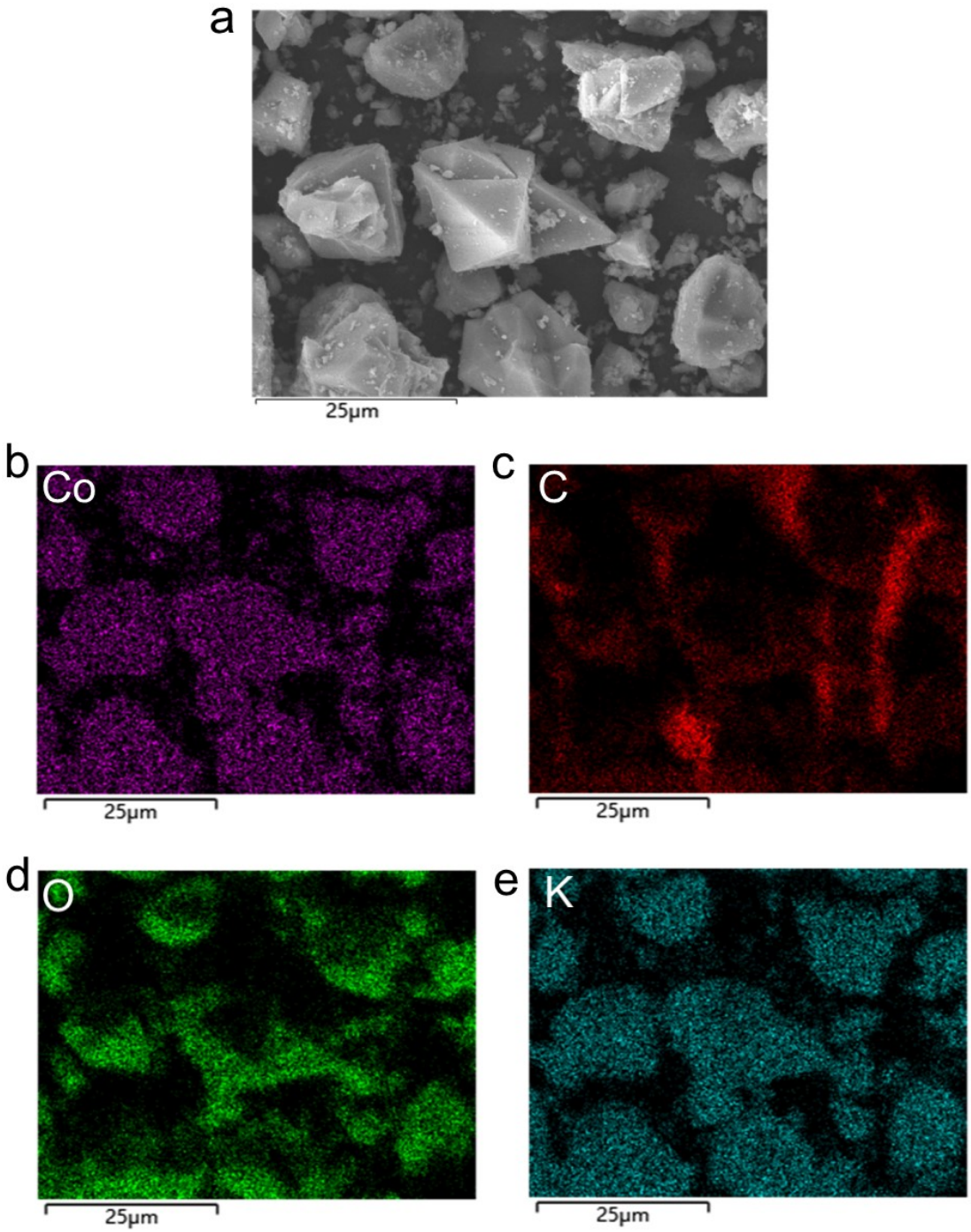

Figure S3. (a) SEM image of UTSA-16. (b-e) EDX mapping of Co, C, O, and K.

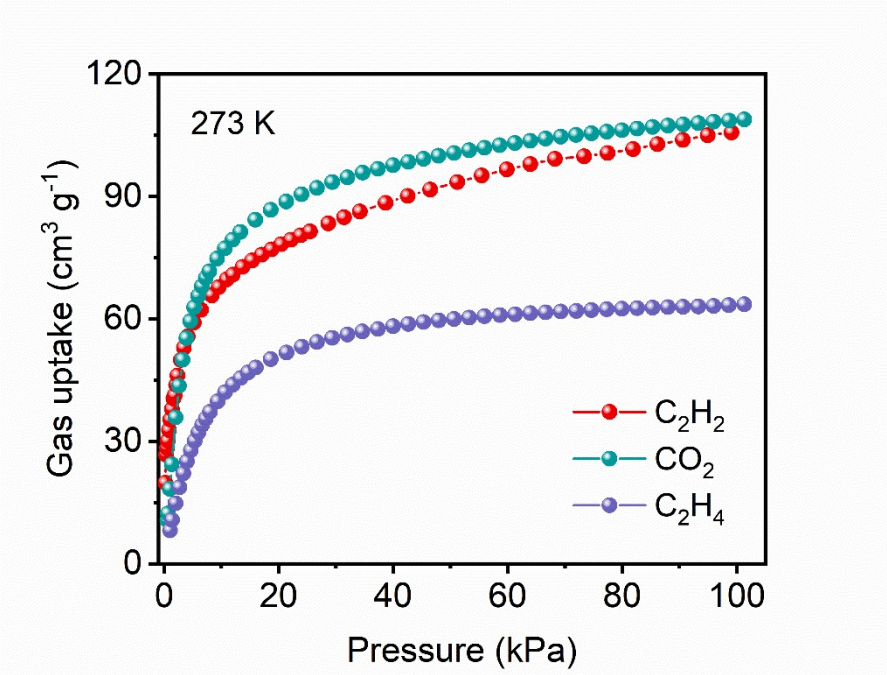

Figure S4. Adsorption isotherms of C_2H_2, CO_2, and C_2H_4 on UTSA-16 at 273 K

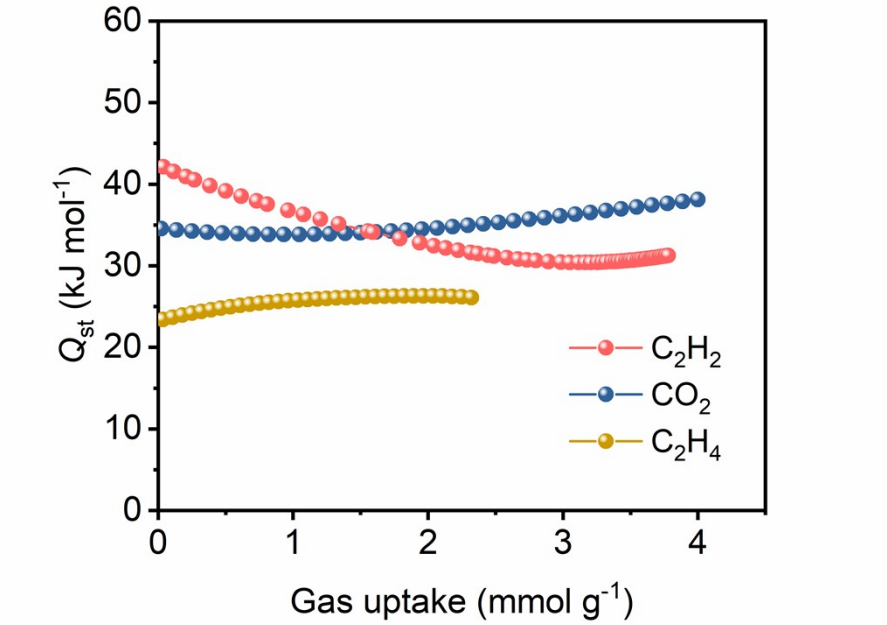

Figure S5. Q_{st} profile of C_2H_2, CO_2, and C_2H_4

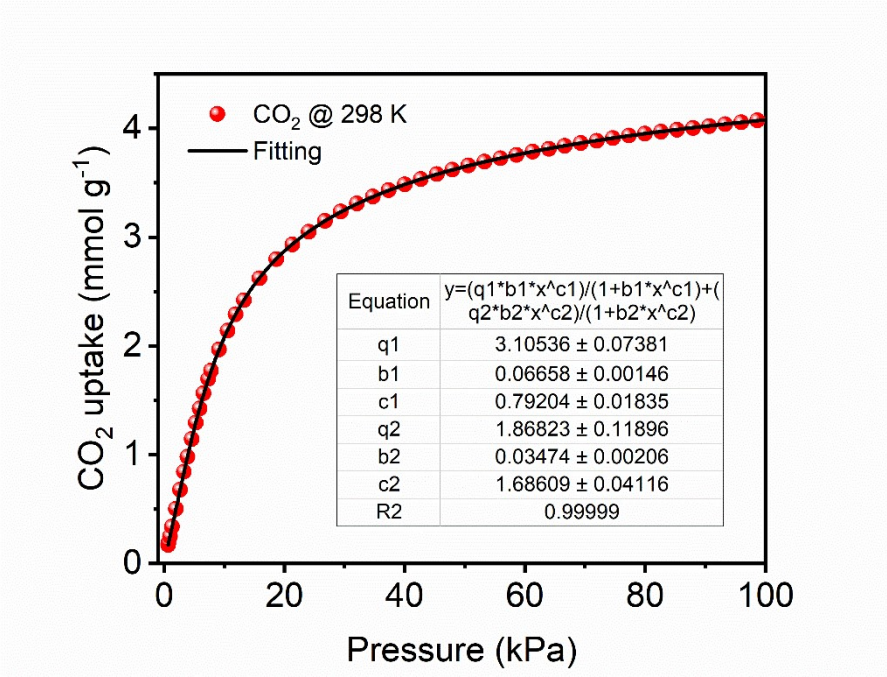

Figure S6. Fitting of CO_2 adsorption isotherm at 298 K with Langmuir-Freundlich equation

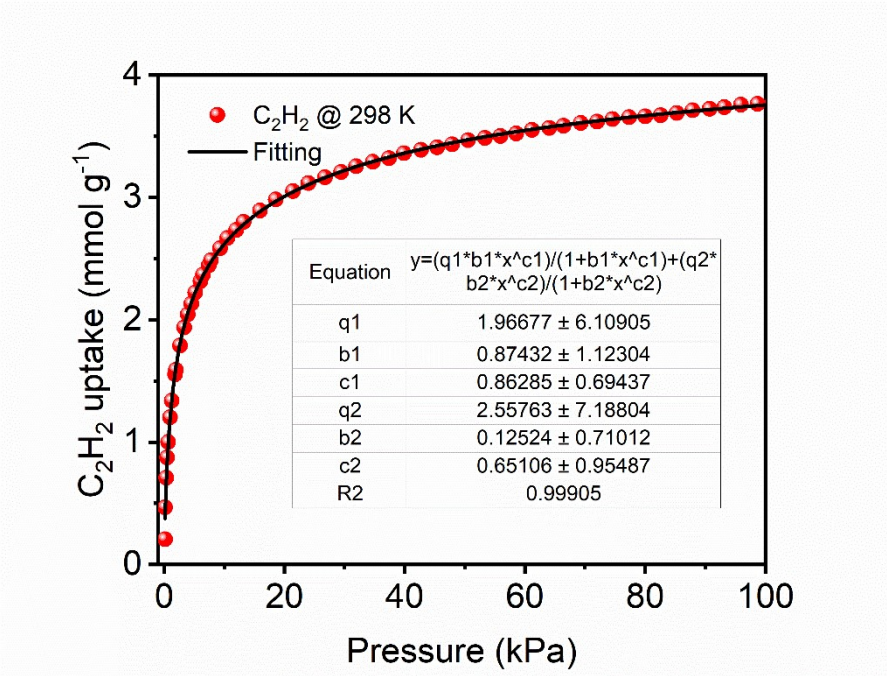

Figure S7. Fitting of C_2H_2 adsorption isotherm at 298 K with Langmuir-Freundlich equation

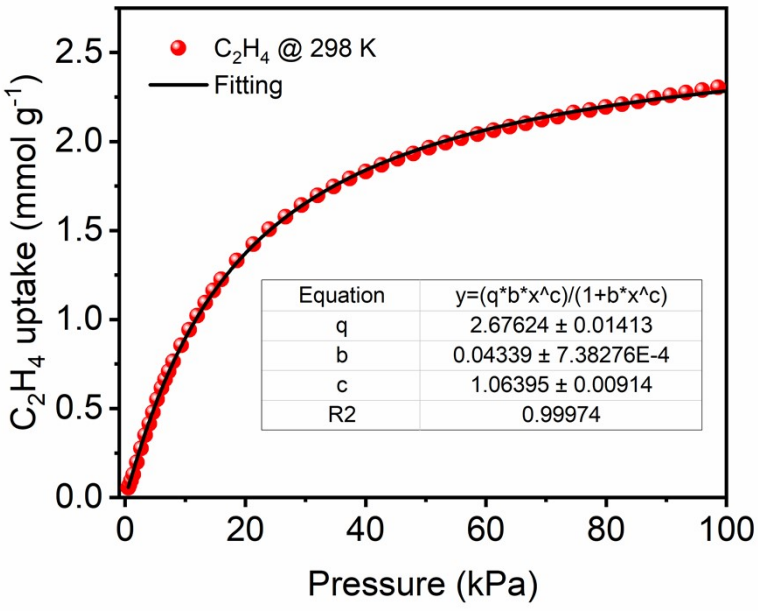

Figure S8. Fitting of C_2H_4 adsorption isotherm at 298 K with Langmuir-Freundlich equation

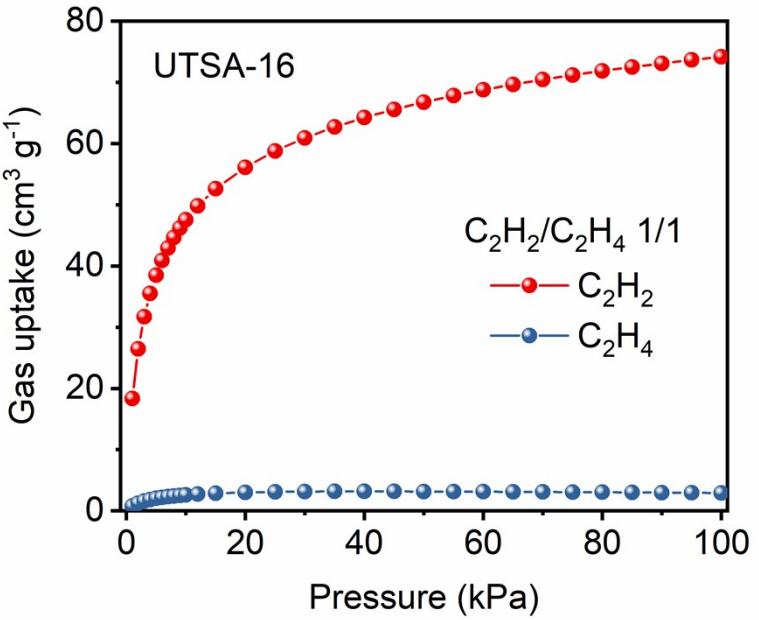

Figure S9. IAST predicted binary adsorption isotherms of equimoalr C_2H_2/C_2H_4 mixture on UTSA-16 at 298 K

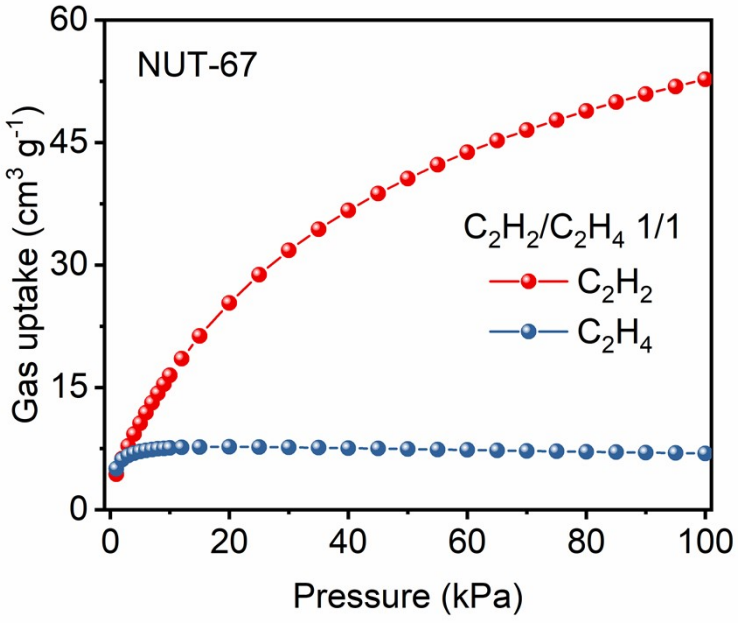

Figure S10. IAST predicted binary adsorption isotherms of equimoalr C_2H_2/C_2H_4 mixture on NUT-67 at 298 K

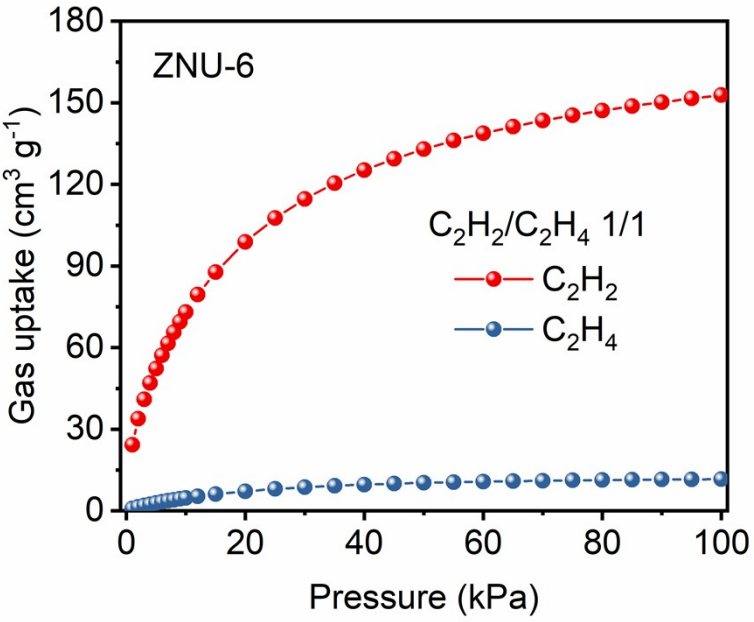

Figure S11. IAST predicted binary adsorption isotherms of equimoalr C_2H_2/C_2H_4 mixture on ZNU-6 at 298 K

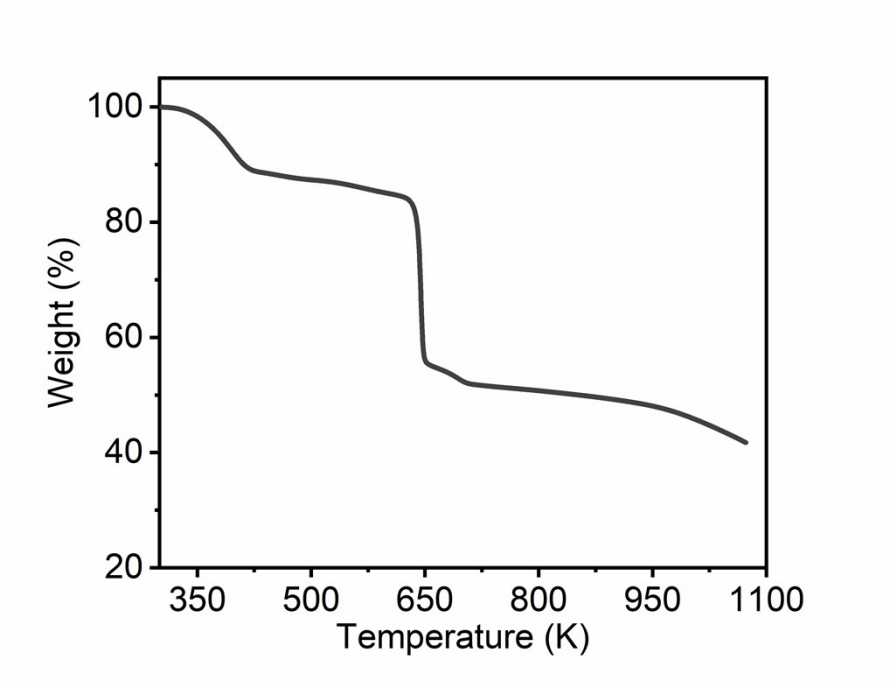

Figure S12. TGA curve of UTSA-16

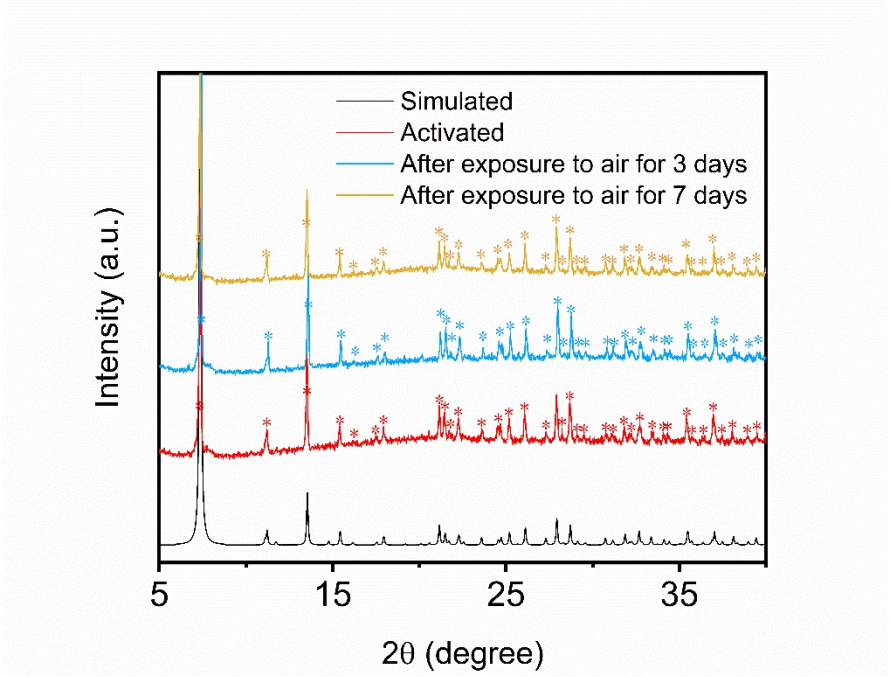

Figure 13. Simulated PXRD pattern and the experimental PXRD patterns of UTSA-16 after different treatments (* refers to characteristic peaks belonging to UTSA-16)

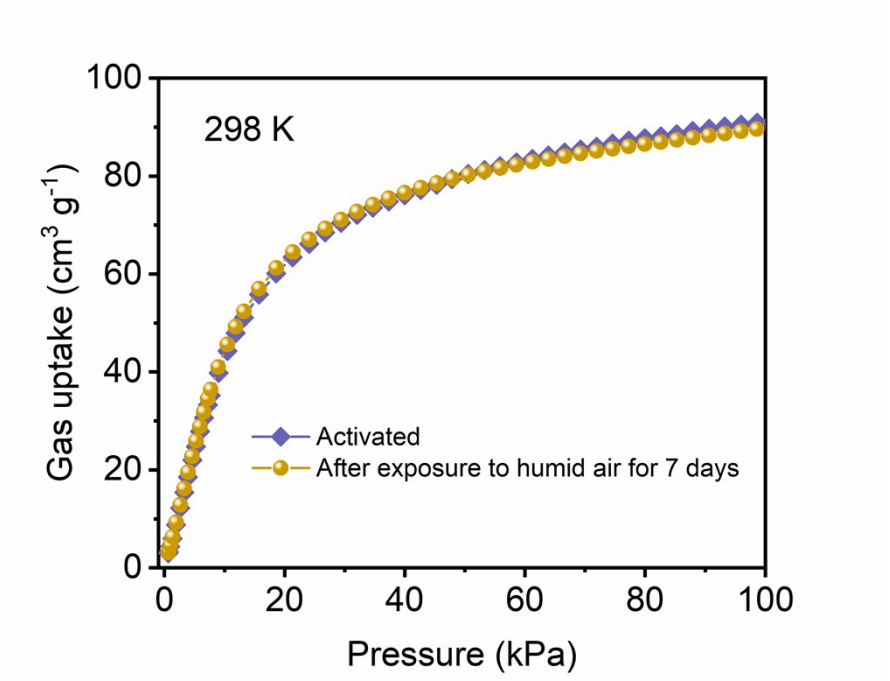

Figure S14. CO_2 adsorption isotherm of activated UTSA-16 and UTSA-16 after exposure to humid air (RH = 70%) for 7 days

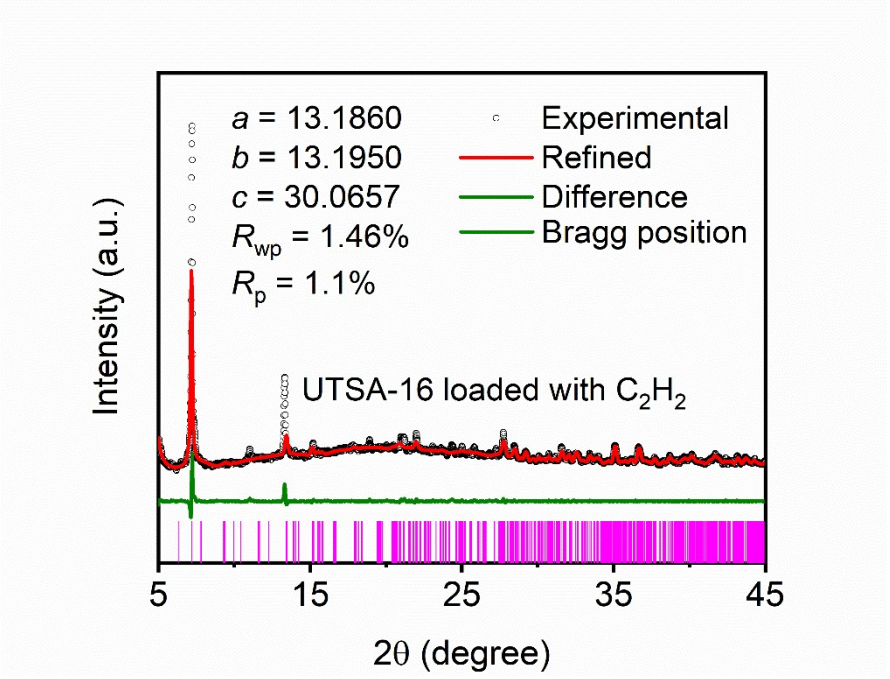

Figure S15. Experimental in situ PXRD pattern and refined PXRD pattern of UTSA-16 loaded with C_2H_2.

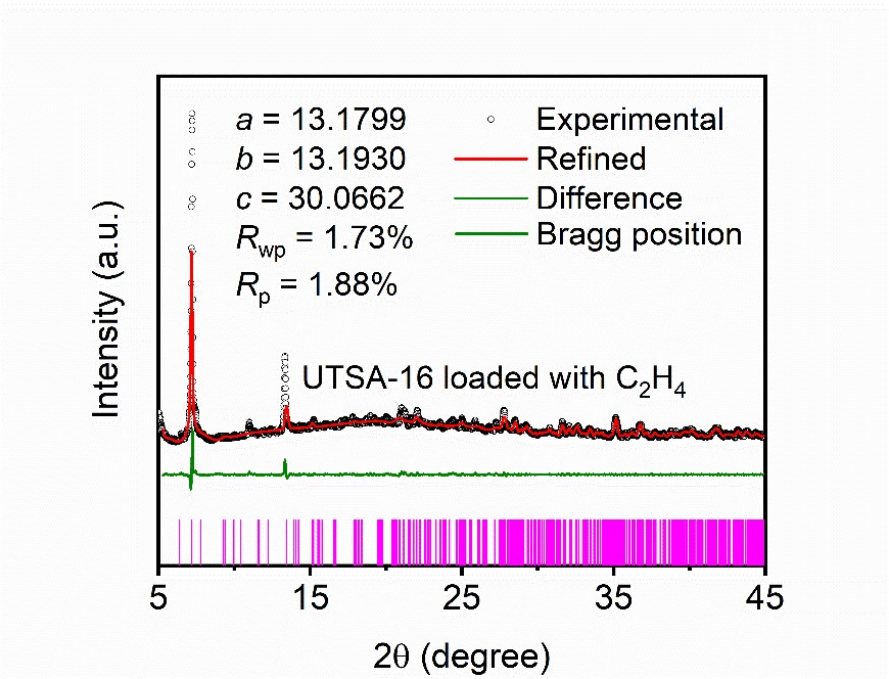

Figure S16. Experimental in situ PXRD pattern and refined PXRD pattern of UTSA-16 loaded with C_2H_4.

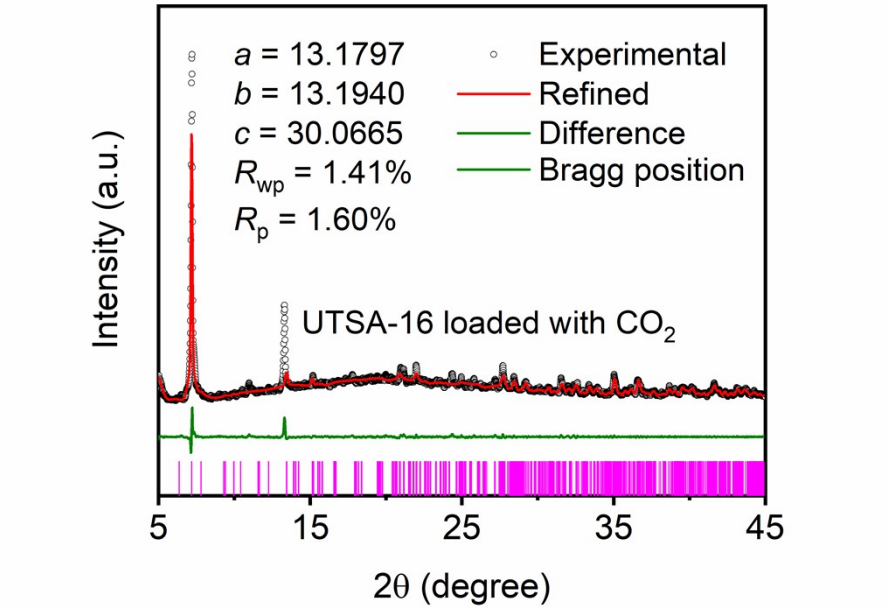

Figure S17. Experimental in situ PXRD pattern and refined PXRD pattern of UTSA-16 loaded with CO_2.

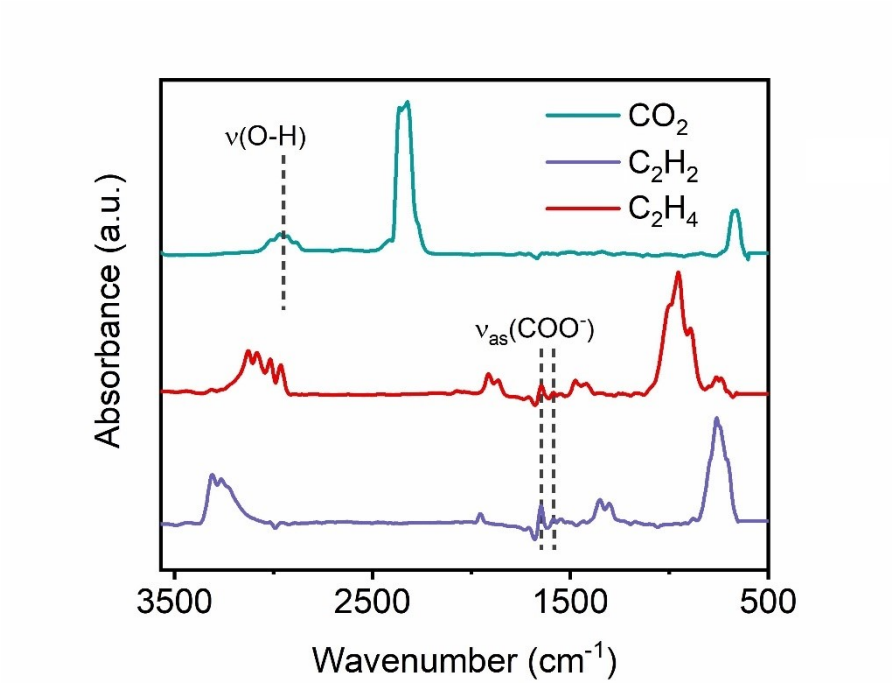

Figure S18. A comparison for the in situ infrared spectra of UTSA-16 loaded with different gases

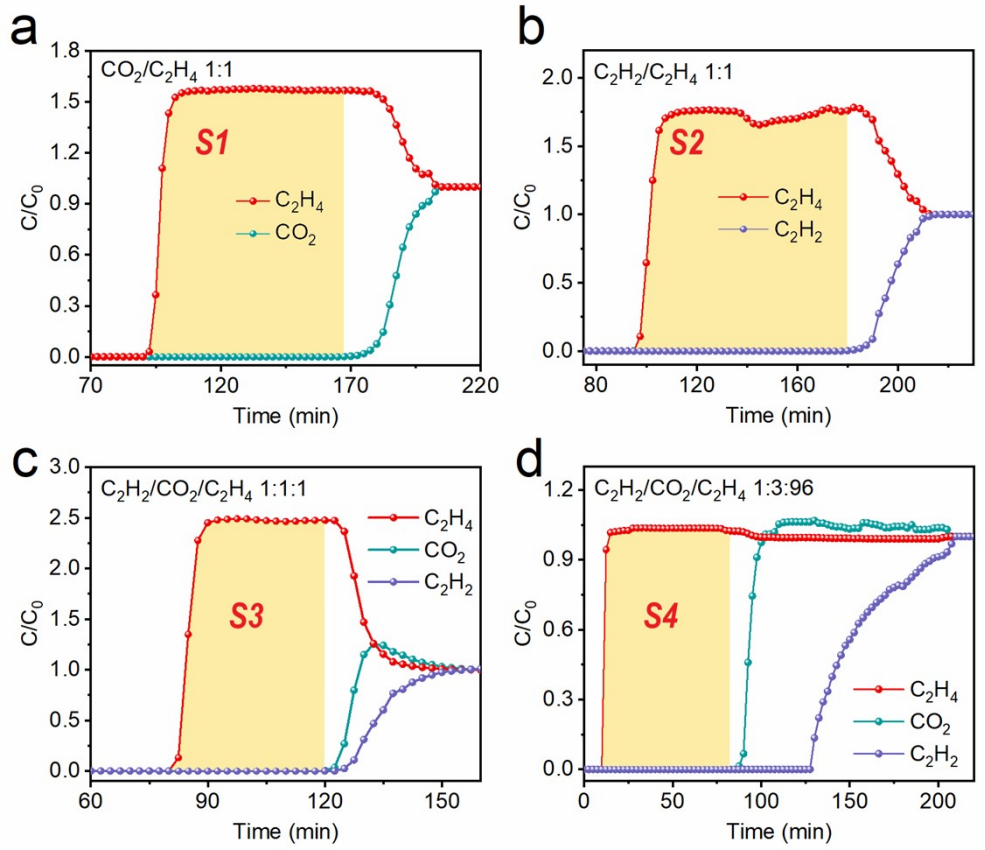

Figure S19. Intergration of breakthrough curves for the calculation of C_2H_4 productivity in different breakthrough tests

$$Q_{C_2H_4} = \frac{v \times V\%}{m} \int_{t_0}^{t_1} (c/c_0) dt = \frac{v \times V\%}{m} \times S$$

For 1/1 CO_2/C_2H_4 mixture:

v = 1 mL min^{-1}, V% = 50%, m = 1.8 g, $S1$ = 103.40 min, $Q_{C_2H_4}$ = 28.7 L kg^{-1}

For 1/1 C_2H_2/C_2H_4 mixture:

v = 1 mL min^{-1}, V% = 50%, m = 1.8 g, $S2$ = 127.78 min, $Q_{C_2H_4}$ = 35.5 L kg^{-1}

For 1/1/1 $C_2H_2/CO_2/C_2H_4$ mixture:

v = 1.5 mL min^{-1}, V% = 33.33%, m = 1.8 g, $S5$ = 98.3 min, $Q_{C_2H_4}$ = 27.3 L kg^{-1}

For 1/3/96 $C_2H_2/CO_2/C_2H_4$ mixture:

v = 10 mL min^{-1}, V% = 96%, m = 1.8 g, $S3$ = 75.60 min, $Q_{C_2H_4}$ = 403.2 L kg^{-1}

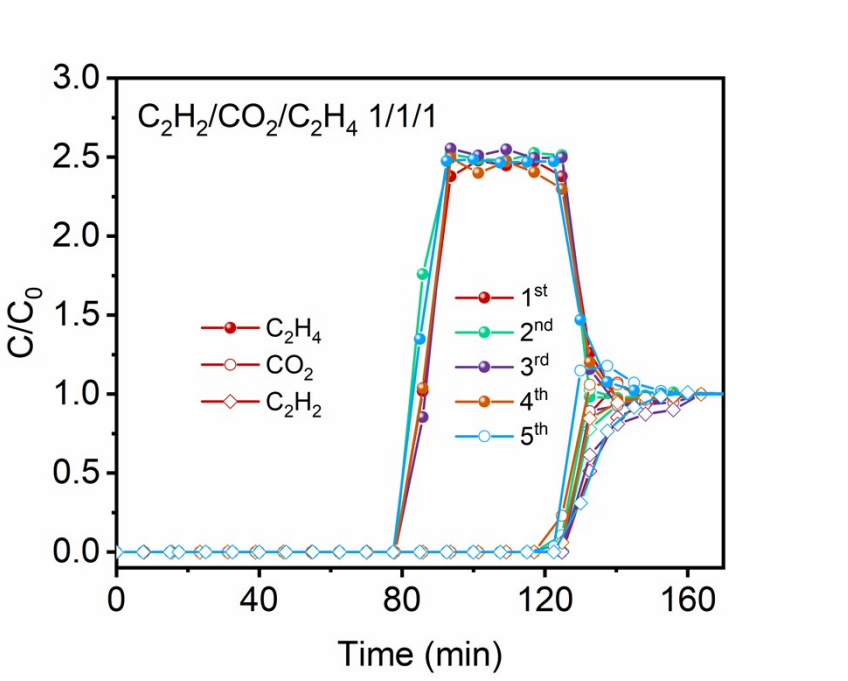

Figure S20. Cyclic breakthrough curves for 1/1/1 $C_2H_2/CO_2/C_2H_4$ mixture at 298 K with a gas flow rate of 1.5 mL min^{-1}

Table S1. Properties of C_2H_2, CO_2, and C_2H_4

	C_2H_2	C_2H_4	CO_2
Molecular size (Å^3)	3.32 × 3.34 × 5.70	3.28 × 4.18 × 4.84	3.18 × 3.33 × 5.36
Kinetic diameter (Å)	3.3	4.2	3.3
Boiling point (K)	189.3	169.5	194.7
Polarizability ($\times 10^{-25}$ cm^3)	33.3–39.9	42.5	29.11

Table S2. Separation data and decomposition temprature of UTSA-16 and other related adsorbents

	Temperature (K)	Gas uptake ($cm^3\ g^{-1}$)				IAST selectivity			Decomposition temperature (K)	Reference
		C_2H_2 at 1 kPa	C_2H_2 at 100 kPa	CO_2 at 10 kPa	CO_2 at 100 kPa	1/99 C_2H_2/C_2H_4	1/1 C_2H_2/C_2H_4	1/1 CO_2/C_2H_4		
UTSA-16	298	28.0	84.7	45.0	91.6	18.3	25.4	5.7	633	This work
ZNU-6	298	34.3	180.5	49.5	106.6	14.3	13.2	3.9	526	2
NUT-67	298	28.2 (7.5 kPa)	73.7	31	44.8	8.1		10.8	523	3
NUT-65	263	16.8	86.2	2	79.3				573	4
SIFSIX-17-Ni	298	20.4	73.9	20	51.5		506		493	5
TIFSIX-17-Ni	298	30.9	73.9	22	47.0		670		533	5
F-PYMO-Cu	298	8.5 (10 kPa)	20.0	14	31.0	192	10^8		503	6

Table S3. Virial fitting parameters of C_2H_2, CO_2, and C_2H_4

	C_2H_2	C_2H_4	CO_2
a_0	-5100.70321	-2800.0023	-4159.39404
a_1	35.48389	-17.28482	4.37354
a_2	-0.52142	0.22197	-0.05505
a_3	0.00927	0.00326	9.75783E-6
a_4	-9.0826E-5	-1.23209E-4	8.38182E-7
a_5	2.79515E-7	9.92177E-7	-2.06276E-9
b_0	15.59128	10.28795	13.57882
b_1	-0.10908	0.05035	-0.01449
b_2	0.00101	-2.20884E-4	1.84234E-4
R^2	0.97229	0.9759	0.99957

Table S4. Langmuir-Freundlich fitting paramters of C_2H_2, CO_2, and C_2H_4 for different materials at 298 K (unit: mmol g^{-1} for q_i, kPa^{-1} for b_i)

Materials	Gas	q_A	b_A	c_A	q_B	b_B	c_B	Reference
UTSA-16	C_2H_2	1.96677	0.87432	0.86285	2.55763	0.12524	0.65106	This work
	CO_2	3.10536	0.06658	0.79204	1.86823	0.03474	1.68609	
	C_2H_4	2.67624	0.04339	1.06395	0	0	1	
ZNU-6	C_2H_2	1.2	4	1	7.6	0.0805	1	2
	CO_2	7.7	0.00593	1	1.8	0.352	1	
	C_2H_4	7.6	0.0162	1	0	0	1	
NUT-67	C_2H_2	4.52918	0.10655	0.67784	8.3E-17	17.9722	2.03715	3
	CO_2	2.34572	0.34121	0.60063	0.00528	0.33899	153.67101	
	C_2H_4	2.28851	0.02331	0.70616	0.4507	3.42358	1.0109	

Table S5. The material cost for the preparation of different materials

Materials	Ingredient	Price ($ kg^{-1})	Ingredient	Price ($ kg^{-1})	Ingredient	Price ($ kg^{-1})	Preparation cost ($ kg^{-1})	Reference
UTSA-16	$Co(OAc)_2 \cdot 4H_2O$	92	KOH	17.63	Citric acid monohydrate	21.6	47.9	This work
ZNU-6	$Cu(NO_3)_2 \cdot 3H_2O$	19.4	$(NH_4)_2GeF_6$	25522	Tri(pyridin-4-yl)amine	98.21	98209	2
NUT-65	$CuSiF_6 \cdot 6H_2O$	1760	1,4-dibromobenzene	62.8	Imidazole	53	2505	4
NUT-67	$CuSiF_6 \cdot 6H_2O$	1760	1,4-dibromobenzene	62.8	Imidazole	53	2505	3
F-PYMO-Cu	$Cu(NO_3)_2 \cdot 3H_2O$	19.4	5-fluoro-2-hydroxypyrimidine	54478			40586	6
SIFSIX-17-Ni	$NiSiF_6 \cdot 6H_2O$	330	2-aminopyrazine	4040			2224	5
TIFSIX-17-Ni	$NiTiF_6 \cdot 6H_2O$	330	2-aminopyrazine	4040			2137	5

Table S6. Experimental dynamic C_2H_4 productivity for different porous materials

Material	Gas composition (C_2H_2/CO_2/C_2H_4)	Temperature (K)	C_2H_4 productivity (L kg^{-1})	Reference
UTSA-16	1/3/96	298	403.2	This work
ZNU-6	1/5/94	298	478	2
NUT-67	0.96/4.04/95.00	298	145	3
F-PYMO-Cu	0.97/3/96.03	298	27	6
NUT-65	0.967/3.33/95.7	263	26	4
SIFSIX-17-Ni	1/1/1	298	7.2	5
TIFSIX-17-Ni	1/1/1	298	15.7	5
UTSA-16	1/1/1	298	27.3	This work

References

1 S. Xiang, Y. He, Z. Zhang, H. Wu, W. Zhou, R. Krishna and B. Chen, Microporous metal-organic framework with potential for carbon dioxide capture at ambient conditions, *Nat. Commun.*, 2012, **3**, 954.

2 Y. Jiang, Y. Hu, B. Luan, L. Wang, R. Krishna, HaofeiNi, X. Hu and Y. Zhang, Benchmark single-step ethylene purification from ternary mixtures by a customized fluorinated anion-embedded MOF, *Nat. Commun.*, 2023, **14**, 401.

3 Q. Dong, Y. Huang, K. Hyeon-Deuk, I.-Y. Chang, J. Wan, C. Chen, J. Duan, W. Jin and S. Kitagawa, Shape- and size-dependent kinetic ethylene sieving from a ternary mixture by a trap-and-flow channel crystal, *Adv. Funct. Mater.*, 2022, **32**, 2203745.

4 Q. Dong, X. Zhang, S. Liu, R.-B. Lin, Y. Guo, Y. Ma, A. Yonezu, R. Krishna, G. Liu, J. Duan, R. Matsuda, W. Jin and B. Chen, Tuning gate-opening of a flexible metal–organic framework for ternary gas seving separation, *Angew. Chem. Int. Ed.*, 2020, **59**, 22756-22762.

5 S. Mukherjee, N. Kumar, A. A. Bezrukov, K. Tan, T. Pham, K. A. Forrest, K. A. Oyekan, O. T. Qazvini, D. G. Madden, B. Space and M. J. Zaworotko, Amino-functionalised hybrid ultramicroporous materials that enable single-step ethylene purification from a ternary mixture, *Angew. Chem. Int. Ed.*, 2021, **60**, 10902-10909.

6 X. Jiang, T. Pham, Q.-Y. Zhang, J.-W. Cao, K. A. Forrest and K.-J. Chen, Molecular sieving of acetylene from ethylene in a rigid ultra-microporous metal organic framework, *Chem. Eur. J.*, 2021, **27**, 9446-9453.